ELSEVIER

Polymer 42 (2001) 577–588

polymer

www.elsevier.nl/locate/polymer

Inorganic particle toughening I: micro-mechanical deformations in the fracture of glass bead filled epoxies

J. Lee[1], A.F. Yee*

Macromolecular Science and Engineering Program, The University of Michigan, Ann Arbor, MI 48109, USA

Received 29 February 2000; received in revised form 16 May 2000; accepted 16 May 2000

Abstract

General characteristics of micro-mechanical deformations found in the fracture of various glass bead filled epoxies are investigated. Among the various types of step features on fracture surfaces, the basic longitudinal texture is not influenced by the existence of glass beads, but most other steps formed are significantly affected. Various microscopic investigations show that microcracking does not extensively occur in the fracture of glass bead filled epoxies. Microcracking other than debonding of glass beads is seldom observed, and furthermore, debonding is found to occur only on and near the fracture surface. Micro-shear bands are clearly identified and distinguished from microcracks found in unnotched tensile specimens. Based on examination of micro-mechanical deformations, three types of fracture processes are proposed for glass bead filled epoxies having different glass bead contents and interfacial strengths.

Keywords: Epoxy; Fracture; Toughening

1. Introduction

Toughening polymers is a continually challenging area for polymer scientists and engineers. Among various successful toughening methods developed for more than four decades, rubber and inorganic particle toughenings are the most popular. Understanding the fracture behavior of the two types of toughened systems, one containing soft (rubber) particles and the other rigid (inorganic) particles, is important not only because these systems have successfully improved toughness, but also because it can provide fundamentals for researches on more complicated blends and composites.

While rubber toughening can provide a dramatic toughness increase, the effect of inorganic particle toughening is more modest. However, inorganic particle toughening has an attractive advantage over rubber toughening, which is that it can also improve modulus. It is generally true in rubber toughening that toughness increase is achieved at the expense of modulus decrease.

The moderate toughness increase achieved by the incorporation of inorganic particles has been explained mainly by the crack front bowing mechanism [1,2]. According to this mechanism, inorganic particles inside the polymer matrix can resist crack propagation. Therefore, a crack front starts to bow out between particles, when it meets the particles. By analyzing the line tension stored along the bowed secondary crack fronts, the toughness increase due to the incorporation of inorganic particles can be assessed. Although some aspects of inorganic particle toughening have successfully been explained by this mechanism [3–8], many of them are still left unexplained. For example, the insignificant effect of surface treatment of glass beads on the fracture toughness of glass beads/thermoset composites has never been understood using the crack front bowing mechanism [1,9]. The limits of this mechanism result from the assumption that inorganic particles have a certain amount of resistance (impenetrability) against crack propagation. (In most studies, perfect impenetrability has been assumed.) Although this mechanism can explain the relationship between the resistance of particles and the macroscopic fracture toughness of composites by analyzing the line tension, it cannot link the resistance and design variables in the preparation of toughened composites. Discovering how inorganic particles achieve a certain degree of resistance against crack propagation (how they can dissipate

* Corresponding author. Fax.: +1-734-763-4788.

E-mail addresses: jong@cems.umn.edu (J. Lee), afyee@engin.umich.edu (A.F. Yee).

[1] Current address: Department of Chemical Engineering and Materials Science, The University of Minnesota, Minneapolis, MN 55455, USA.

0032-3861/01/$ - see front matter
PII: S0032-3861(00)00397-9

extra fracture energy and toughen polymer matrices) seems to be more essential in understanding inorganic particle toughening and developing future toughened composites.

We first started phenomenological studies on the effect of material variables on micro-mechanical deformations, and their results were reported elsewhere [10–13]. The micro-mechanical deformations could dissipate a significant amount of fracture energy. In these series of studies, glass bead filled epoxies were used as model systems for inorganic particle toughened polymers. In our previous phenomenological studies, the effect of material variables such as inherent matrix toughness and cleaning process of glass beads on micro-mechanical deformations explored. Contrary to the common generalization about inorganic particle toughening [1,9], the fracture of glass bead filled epoxies was found to have noticeable ductile characteristics, e.g. diffuse shear yielding and micro-shear banding of matrix. As a whole, four types of micro-mechanical deformations including step formation, debonding of glass beads, diffuse matrix shear (DS) yielding, and micro-shear (MS) banding were found to be the major ones that can be found in the fracture of glass bead filled epoxies.

In this study, the micro-mechanical deformations were studied in depth using the same glass bead filled epoxies as previously prepared and studied in Ref. [10–13]. Understanding the general properties of the deformations is the main objective in this study (part I) and it is basic knowledge for the correlation studies in the following part II. Eventually, these two studies enable us to establish the major toughening mechanisms of glass bead filled epoxies.

2. Experimental

Glass bead filled epoxies were prepared from diglycidyl ether of bisphenol A (DGEBA) resins, 4,4′-diaminodiphenylsulphone (DDS), and Spheriglass® A-glass beads (soda-lime) as described in the previous publications [10–13]. Four types of DGEBA resins, DER® 332 ($M_w = 343$), 661 ($M_w = 1050$), 664 ($M_w = 1850$), 667 ($M_w = 3600$), and two kinds of glass beads, SG (mean diameter = 3.3 μm) and LG (mean diameter = 24.4 μm) were used. The numbers in the commercial names of DGEBA resins will be used as the designations of epoxy matrix, e.g. 661. The basic physical properties of materials, and the experimental details of composite preparation and basic characterizations (fracture toughness measurement, double-edge-notched four-point bend (DEN-4PB) technique, scanning electron microscopy (SEM), optical microscopy (OM), and petrographic thin-sectioning technique) are available in the previous publication [10–13]. For the assessment of fracture toughness, single-edge-notched (SEN) specimens (thickness = 6.35, width = 12.7, and span = 50.8 mm) were fractured in three-point bend (3PB) geometry. A screw-driven Instron machine (Instron 4502) was used at a crosshead speed of 2.54 mm/min. The DEN-4PB technique produced sub-critically loaded cracks, which were examined using the petrographic thin-sectioning technique.

In situ observation of the surface of SEN samples fracturing in the 3PB geometry was made using a Nikon Microphot II microscope. The same kinds of glass bead filled epoxies used for the fracture toughness assessment were cut into $6.35 \times 12.7 \times 50.8$ mm^3. The surface of samples was carefully polished following the petrographic thin-sectioning technique [14–16]. After creating sharp initial notches following the method described in Ref. [10–13], samples were fractured on the sample stage of the microscope at an arbitrary strain rate driven by hand. A series of surface events, which occurred during fracture, was observed.

For an investigation on a cryofractured surface, samples of about 2 to 4 mm thickness were immersed in liquid nitrogen for more than an hour and then fractured in liquid nitrogen.

The brittle fracture surface of epoxies exhibits a basic longitudinal texture (BLT) [17,18], which is thought to give rise to toughening effect. For the analysis of BLT, three different microscopy techniques were used to cover a wide range of magnification: atomic force microscopy (AFM), SEM, and OM. For AFM, a Digital Instruments NanoScope III equipped with an etched silicon probe (Digital Instrument TESP) was used. The analysis at the lowest magnification was performed by using a reflected light optical microscope (Nikon Microphot II). Plot profiles showing the gray scale (0–256) of digitized images (600 dpi) were obtained using a commercial software (NIH image). This software was also used to obtain the power spectrum, i.e. the 2D plot of the Fast Fourier transform of the image [19]. The power spectrum was quantitatively analyzed to obtain the characteristic periodicity of basic longitudinal texture (BLT) [17]. For each composition, more than 5 different regions (size $= 1.6 \times 10^3$ μm^2) in micrographs were examined, and the average value of spatial frequency showing a peak in the plot profile of the power spectra (see Fig. 3) was taken as the characteristic periodicity of BLT.

The effect of thermal energy on the micro-mechanical deformations in the thin-sections of fractured or sub-critically damaged specimens was studied using an Olympus BH-2 optical microscope and a Mettler EP 82 hot stage. While a thin-section was heated on the hot stage at 0.5°C/min, changes in micro-mechanical deformations in the section were observed. Transmission electron microscopy (TEM) was also carried out on ultramicrotomed thin sections using a JEOL JEM-2000FX Analytical Electron Microscope. For TEM observation, thin sections of ca. 60 nm thickness were prepared by microtoming DEN-4PB and SEN-3PB samples using a Reichert-Jung Ultracut E microtome at room temperature.

3. Results and discussion

Before the micro-mechanical deformations in process zone, which could dissipate fracture energy, are discussed,

the precise definition of process zone must be established. The process zone is a region where sub-critical (stable) crack growth occurs [14,20]. This region ranges from an initial crack tip to the onset point of unstable crack propagation, where the fast-fracture region starts. Instability in crack propagation occurs when the following two requirements are met:

$$G - R \geq 0 \qquad \text{and} \qquad \mathrm{d}G/\mathrm{d}A > \mathrm{d}R/\mathrm{d}A \tag{1}$$

where G is the energy release rate, R is the fracture resistance of materials, and A is the fracture area [20]. Therefore, the process zone size depends on the changes of G and R with increase of A.

In SEN-3PB specimens used in the current experiment, sub-critical crack growth occurs in a very limited area, i.e. the process zone. While a crack front is moving in this zone, the fracture resistance of materials significantly increases. Since G_{IC} (or K_{IC}) is measured at the onset point of unstable crack propagation, micro-mechanical deformations occurring in the process zone are important for understanding the sources of toughness.

In various microscopy studies, several micro-mechanical deformations have been found in the process zone, which occur during the fracture of glass bead filled epoxies. All of these deformations can be categorized into three groups: step formation, debonding/diffuse matrix shear (DS) yielding, and micro-shear (MS) banding. Debonding of glass beads and DS yielding of matrix can be treated as a combined process because the former was found to be always accompanied by the latter in the previous studies [10–13]. The debonding of glass beads was thought to trigger DS yielding. In this study, microcracking including debonding, which has been proposed as one of toughening mechanisms of glass bead filled epoxies [21–23], is investigated.

3.1. Step structures

The fracture surface of any material is not perfectly smooth; it is rough on all scales [24,25]. Several kinds of step structures contributing to the roughness can be observed on fracture surface, viz. characteristic tail structure behind glass beads [3,26,27], ‘lance’ [28,29], basic longitudinal texture (BLT) [17,18], etc. The characteristic tail structure and the ‘lance’ can be observed at a lower magnification than the basic longitudinal texture. The ‘lance’ is also called either ‘river’ or ‘hackle’ [29–35], but sometimes these nomenclatures refer to different features [29].

Fig. 1 shows the typical surface topology of glass bead filled epoxies. The dark spheres in these micrographs are glass beads. A large step parallel to the direction of crack propagation can be seen behind the glass bead in the center of the micrograph (A). This is the characteristic tail structure [3,26,27] formed when two secondary crack fronts separated by a glass bead meet with each other. Besides the characteristic tails, many kinds of steps, particularly ‘lance’, ‘river’, and ‘hackles’, can also be found in the

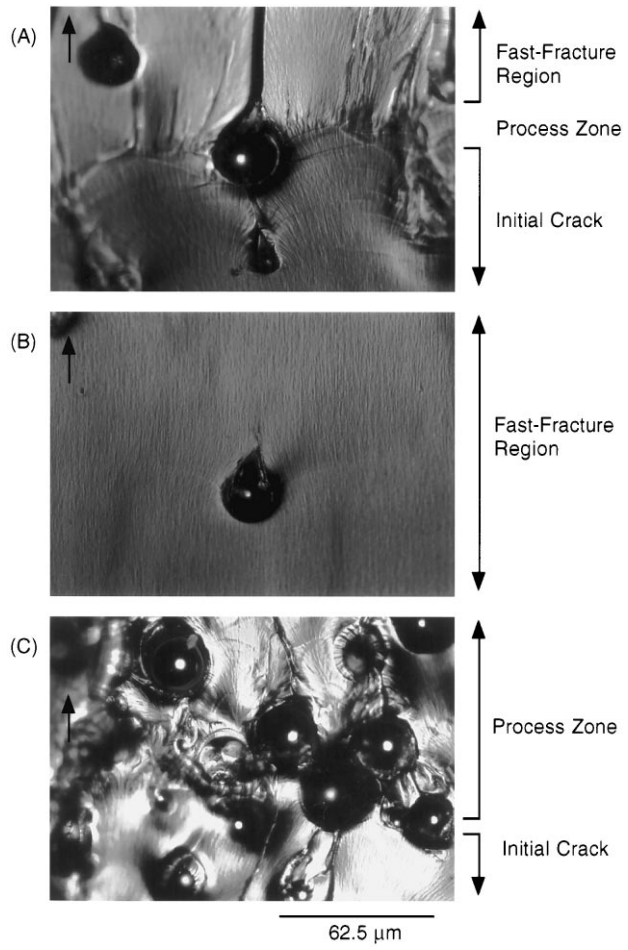

Fig. 1. Reflected light optical micrographs of fracture surface of SEN-3PB specimens: (A) and (B) 5 vol% LG/661; (C) 20 vol% LG/661. The arrows inside micrographs indicate the direction of crack propagation.

OM and SEM micrographs of fracture surfaces, most of which are thought to be formed due to mixed mode fracture in a constrained crack propagation situation [28,32–35].

Besides the steps discussed above, there are slightly curved line features roughly perpendicular to the direction of crack propagation in Fig. 1(A). These lines were formed where crack fronts are arrested for a certain period of time and break away upon further loading. The small angle between two crack planes behind and ahead of a crack arrest line renders this line visible on the fracture surface. When the glass bead content is relatively low (usually less than 5 vol%), only a few but distinct crack arrest lines are visible, as can be seen in Fig. 1(A). In this case, the process zone is confined within a small region around the crack arrest lines having a few glass beads. As glass bead content increases, more crack arrest lines become visible in the process zone, and the directions of the lines become more irregular (Fig. 1(C)). The irregular directions show that the directions of local crack propagation in the process zone are not always the same as that of macroscopic crack propagation. This is mainly due to the secondary crack fronts generated by glass beads ahead of primary crack tips. In contrast to

Fig. 1(A) and (C), the micrograph Fig. 1(B) does not show any distinct crack arrest line. This is because a crack front can hardly be arrested in the fast-fracture region.

In addition to the relatively large steps described above, there is another kind of fine step structure parallel to crack propagation direction in Fig. 1, i.e. basic longitudinal texture (BLT). It has been reported [17,18,36] that this texture is visible on the fracture surface of all brittle polymers, and its wavelength (periodicity) is approximately 0.2 to 1 μm. Interestingly, the wavelength of the textures in Fig. 1 seems to be larger than 1 μm. Because BLT is always parallel to the crack propagation direction [17,18], the direction of local crack propagation can be traced by an examination of BLT. The BLT shows that the crack fronts were bowed out between glass beads during fracture as the crack arrest lines in Fig. 1 show. The crack front bowing can also be found around the characteristic tails and 'lances' [37]. These results conclusively prove that crack front bowing is present during fracture in these particulate composite systems.

Both crack arrest lines and BLT can also be found in SEM micrographs (Fig. 2), but they are not observed as clearly as in OM micrographs (Fig. 1). While characteristic tails and 'lances' are clearly noticeable, crack arrest lines and BLT are not visible in Fig. 2(A). A horizontal (slightly curved) line perpendicular to the direction of crack propagation exists in the middle of the micrograph Fig. 2(A), which is a crack arrest line. This blurred crack arrest line becomes more distinct in the magnified micrograph Fig. 2(B). The crack arrest line is inclined at about 30° from the horizon of the micrograph Fig. 2(B), and the directions of BLT above and below this line are significantly different. The two fracture surfaces above and below this line have different levels of brightness, because they are inclined at different angles to the electron beam. The periodicity of BLT is rather difficult to notice in this micrograph, but periodicities of approximately 2–3 μm and ≥1 μm can be observed in Fig. 2(B). Fig. 2(C) is a plot of the gray scale of digitized image versus the *y*-direction of a selected area (C) in the micrograph Fig. 2(A). Although the existence of a crack arrest line is not clear in the micrograph Fig. 2(A), the plot profile shows a deflection in the middle of the selected area Fig. 2(C), which results from the existence of the crack arrest line.

An interesting observation is that the crack arrest line seems to be unrelated to the existence of BLT. At the high magnification views (Fig. 2(B)), the crack arrest line is straight. Therefore, the crack front should also be straight in the region of the crack arrest line. This finding can make the fingering hypothesis open to question, which was proposed [17] to explain the formation mechanism of BLT. The hypothesis was also used to explain craze propagation [38–40]. According to the hypothesis, the existence of a liquefied region at the crack tip enables the meniscus instability mechanism [17] to operate during crack propagation, resulting in crack front fingering. If the fingering mechanism occurs during crack propagation [17], the crack front will be wavy.

Robertson et al. first used the terminology, BLT, and

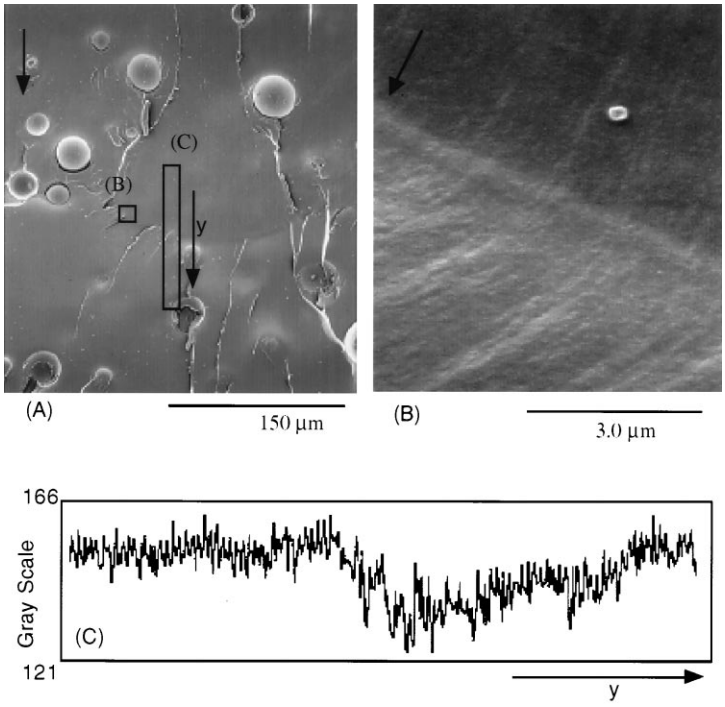

Fig. 2. SEM micrographs of a crack arrest line on the fracture surface of a SEN-3PB specimen of 10 vol% LG/661: (A) process zone; (B) higher magnification micrograph of a region in (A); and (C) plot profile (gray scale 0–256) of a region in (A). The arrows inside micrographs indicate the direction of crack propagation.

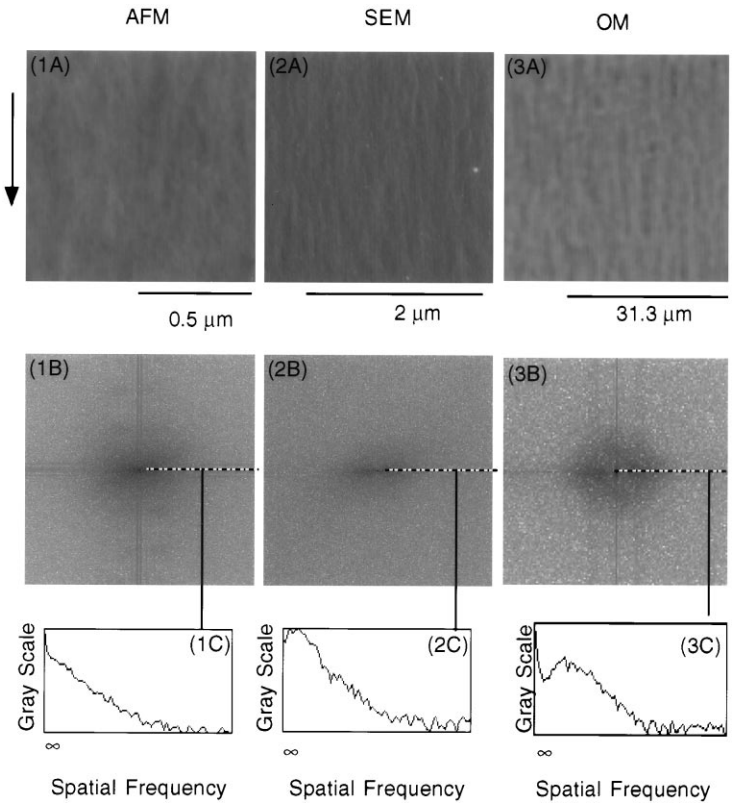

Fig. 3. Basic longitudinal texture on the fracture surface of 10 vol% LG/661: (1) AFM micrograph data; (2) SEM micrograph data; and (3) OM micrograph data; (A) micrographs; (B) power spectrum of Fourier transform of A; (C) plot profile along the half equatorial line of B. The arrows indicate the direction of crack propagation.

studied the relationship between the periodicity of BLT and material properties [17,41]. While the SEM micrographs of only one magnification were used in their studies, in this experiment, three microscopy techniques, AFM, SEM, and OM, were used to observe textures at a wide range of magnifications. This is important because the topology of fracture surfaces can have fractal-like (self-consistency at different scales) structures [24,25].

Fig. 3 shows typical micrographs of fracture surfaces and their Fourier transforms. The power spectra of Fourier transforms are similar to the X-ray diffraction image in reciprocal space [19]. To make observations of the power spectra easier, the plot profiles of the half-equatorial lines in the power spectra were obtained. Thus, in the plot profiles, Figs. 1(C), 2(C), and 3(C), the *x*-axis is the reciprocal periodicity of BLT, and the *y*-axis is the population of textures in arbitrary units.

In Fig. 3, BLT seems to have a fractal-like characteristic. There is still a specific periodicity of about 1–3 μm, which is the most intense in the plot profile Figs. 2(C) and 3(C). This periodicity is designated as the characteristic periodicity of BLT. It should be noted that the characteristic periodicity found in this experiment is significantly larger than that previously reported by Robertson and co-workers [17,18,41].

In an attempt to establish the relationship between the characteristic periodicity and material parameters, the characteristic periodicity of unmodified and glass bead filled epoxies versus epoxide molecular weight is plotted in Fig. 4. The error range in this plot is the range between the maximum and the minimum values measured by using

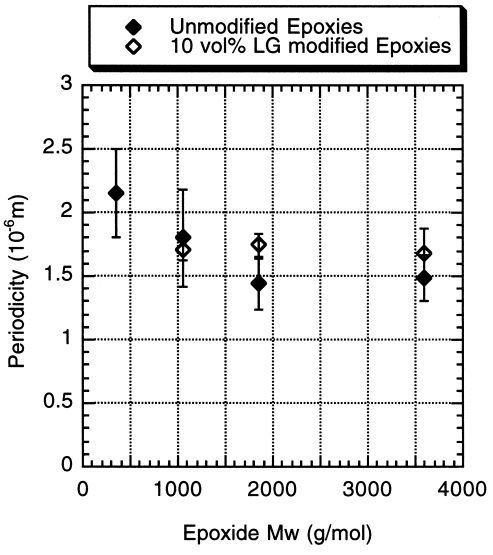

Fig. 4. Characteristic periodicity of basic longitudinal texture versus the epoxide molecular weight of matrices.

the plot profiles of four power spectra. Fig. 4 shows no significant dependence of the periodicity on the existence of glass beads. While the addition of glass beads into epoxy resins does not influence the characteristic periodicity, different epoxy matrices seem to have slightly different characteristic periodicities. When epoxide molecular weight is below 2000 g/mol, the characteristic periodicity seems to decrease slightly with increasing epoxide molecular weight. Above 2000 g/mol, the periodicity may be independent of epoxide molecular weight. However, the differences among the values in Fig. 4 are not large enough to establish a significant trend. Future studies are definitely needed.

3.2. Microcracks — types of microcracks

Three different types of microcracks can be generated in the fracture of glass bead filled epoxies: (1) microcracks in the matrix; (2) in the glass beads; and (3) along the interface between glass beads and the matrix (debonding). Among the three types, the second was not commonly observed in our SEM studies [10–13]. On very rare occasions, fractured glass beads were found both among the glass beads on the fracture surface of composites, and among the glass beads for the preparation of composites before they were mixed with epoxides. Consequently, it is believed that the very rare second type of microcracks result not from the fracture of composites but from the preparation of glass beads, such as the cleaning and the sieving processes [10–13].

In situ observation of the surface of fracturing specimens using SEM has been used to directly investigate the fracture processes of glass bead filled epoxies [42,43]. However, the limitations of this approach must be taken into account when interpreting the results. The fracture process on a specimen surface is not necessarily indicative of the process inside the specimen, because of possible surface defects and a different stress condition (plane stress). In the current experiment, the results obtained by using a similar in-situ technique, i.e. a reflected light OM instead of SEM, are given in Fig. 5(A) and (B). In these OM micrographs, glass beads look darker than the matrix, and the cracks look completely dark.

In Fig. 5(A) and (B), as fracture progresses, the total number of microcracks obviously increases. Contrary to the discussion above, all three types of microcracks can be observed in these micrographs. Microcracks running inside glass beads are just artifacts of specimen preparation, as mentioned above. Furthermore, since sub-surface microcracks of any type are rarely found in the microscopy study of Fig. 6, the significant number of microcracks in matrix and along the particle-matrix interface in Fig. 5 seem to be also artifacts.

Debonding of glass beads is difficult to detect by OM observation on thin-sectioned specimens, because a debonded region is not always discernible. A debonded region appears dark due to destructive interference if the gap between the glass bead and the matrix is within a certain

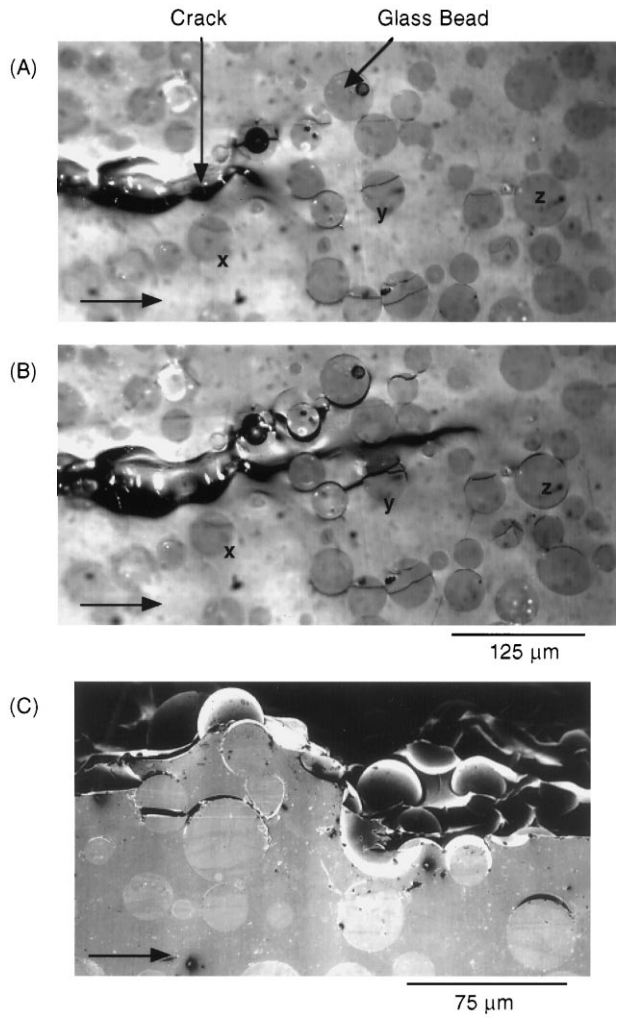

Fig. 5. Fracture process at the polished surface of a SEN-3PB specimen of 30 vol% LG/661: (A) initial appearance before loading (reflected light optical micrograph); (B) appearance of the same area after some crack propagation (reflected light optical micrograph); and (C) after complete fracture (SEM micrograph). The arrows indicate the direction of crack propagation.

range (about 0.3–1.4 μm for visible light) [44]. Therefore, it cannot definitively be confirmed by OM studies whether the debonding (interfacial failure) of glass beads can generally occur beneath a fracture surface as found in Fig. 5. This is the reason why an investigation on the surface cryofractured perpendicular to the original fracture surface was performed. If glass beads beneath the original fracture surface debond from matrix during crack propagation, debonded glass beads must be visible on a cryofractured surface.

Fig. 6 shows typical SEM micrographs of a cryofractured and an original fracture surface. On the original fracture surface generated during the SEN-3PB fracture toughness test, debonded glass beads can clearly be discerned. On the other hand, the cryofractured surface shows no debonded glass beads. Even more than 20 cryofractured specimens showed the same result. It follows that only the glass

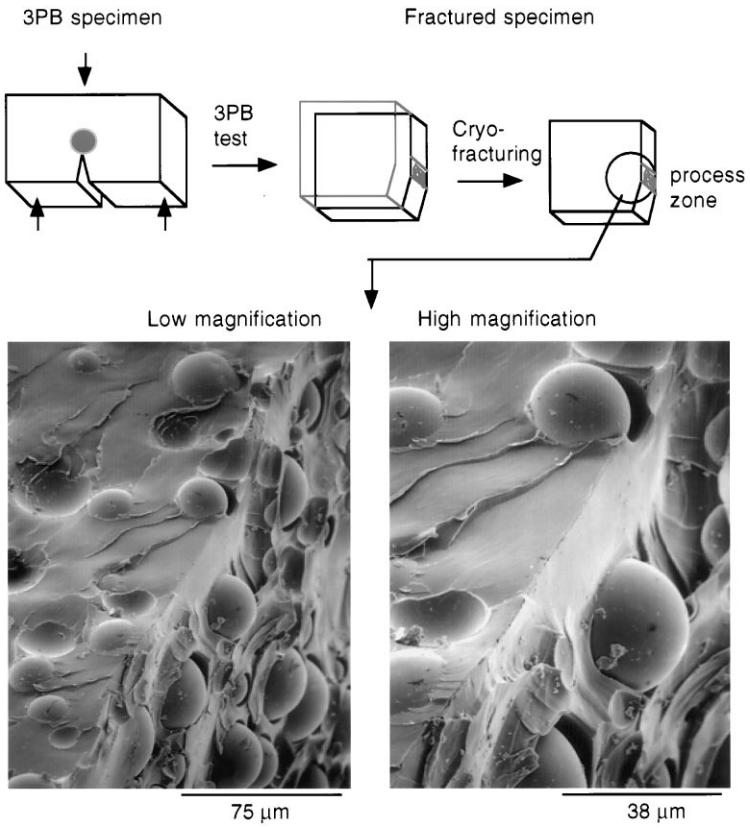

Fig. 6. SEM micrographs of a cryofractured SEN-3PB specimen of 30 vol% LG/661. The original fracture surface (process zone) from the SEN-3PB test is the right side, and the cryofractured surface perpendicular to the original fracture surface is the left side.

beads on a crack propagation path can debond from the matrix. Likewise, microcracks in the matrix and in glass beads were not found beneath the original fracture surface.

This result is important because it can enable us to estimate the contribution of the toughening mechanisms related to microcracks. Several researchers suggest that the debonding of glass beads is one of the major toughening mechanisms [21,23] or is a mechanism, which triggers matrix plastic deformation [45]. The debonding of glass beads, which is found to be the most prominent mode of microcracking in glass bead filled epoxies, can reduce the crack driving force resulting in toughening [22,23,46,47]. The debonding/matrix plastic deformation theory is based on a concept similar to the rubber toughening mechanism (cavitation of rubber particles/matrix shear yielding) [14,48–50]. However, the results presented above show that the volume fraction of microcracks is not large enough to consider microcracking as the major toughening mechanism. Using the same reasoning, the debonding/matrix plastic deformation mechanism cannot be considered to be the major mechanism.

3.3. Microcracks — debonding process

The debonding of glass beads is not a simple process. According to the position on the glass bead surface, debonding can occur under normal or shear stress. Thermal residual misfit between glass beads and the matrix can also affect the debonding process. Fig. 7 shows a complexity found in debonding. Glass beads used in this experiment have a certain range of size distributions [10–13], and according to their size, debonded glass beads have different structures of gaps. Most large glass beads (usually larger than 5–10 μm) in the process zone are clearly debonded from the matrix, having fully grown gaps (Fig. 7(A)). However, most small glass beads are only partially debonded from the matrix, having the drawn fibril-like structure of the matrix in the gaps, as can be seen in Fig. 7(B). The fully-grown gap probably results through drawing the epoxy matrix into fibril-like structure followed by rupture of the drawn structure. Thus, the partially grown gap in Fig. 7(B) might be an intermediate step. The bulged parts of the matrix around debonded glass beads in Fig. 7(A) show that plastic dilatation of the matrix accompanies debonding.

The drawn structures could result from two causes. One is that crack propagation at the equatorial regions of glass beads showing the structures is mixed mode, not pure mode I. (The equatorial region refers to the interfacial region between glass beads and the matrix parallel to the direction of the far-field stress.) This is because the angle between the directions of crack propagation

and the far-field stress is not 90°, and furthermore, the modulus mismatch between glass beads and the matrix is significant [51–54]. Mixed mode stress states usually enhance matrix plastic deformation. The other reason is that the local cross-link density of the epoxy matrix near glass beads may be different from that of the rest of the matrix. The glass bead surface might be able to retard the reactions of epoxides with amines, resulting in a decrease in the local cross-link density. Based on previous studies of crazing in polymers [38,39,40,55], it can be expected that the drawn structures more easily form as the cross-link density decreases. The local cross-link density very near the glass bead surface has never been measured, but there is a report showing that the cross-linking kinetics of epoxy resins can be altered due to the existence of glass beads [56,57].

Next, it must be shown why the debonding process depends on the size of glass beads as shown in Fig. 7. Although the debonding process is quite complex, simple equations were proposed to predict the critical strain (e_i) or stress (σ_i) necessary to cause debonding:

$$e_i^2 = 8\pi G_a/3krE \sin^2 q \qquad [58] \tag{2}$$

$$\sigma_i = -\sigma_t + 2G_aG_o/|\sigma_t|kr \qquad [59] \tag{3}$$

where G_a is the bond fracture energy per unit of bonded surface, k is a constant, E is Young's modulus of composites, q is angle from the pole to a position on a glass bead, r is radius of the glass bead, G_o is shear modulus of the matrix, and σ_t is thermal stress. Although these equations cannot precisely predict e_i and σ_i, they show the basic relationship between $e_i(\sigma_i)$ and r: as the size of a glass bead decreases, the critical stress or strain necessary to cause debonding increases, resulting in more difficult debonding. This is because stored strain energy before debonding depends on r^3, but the energy release due to debonding depends on r^2 instead [58,60,61]. Therefore, in view of these analyses on debonding, the size dependence of the debonding process (Fig. 7) is not surprising.

3.4. Existence of micro-shear bands

One important result from the current experiments is that

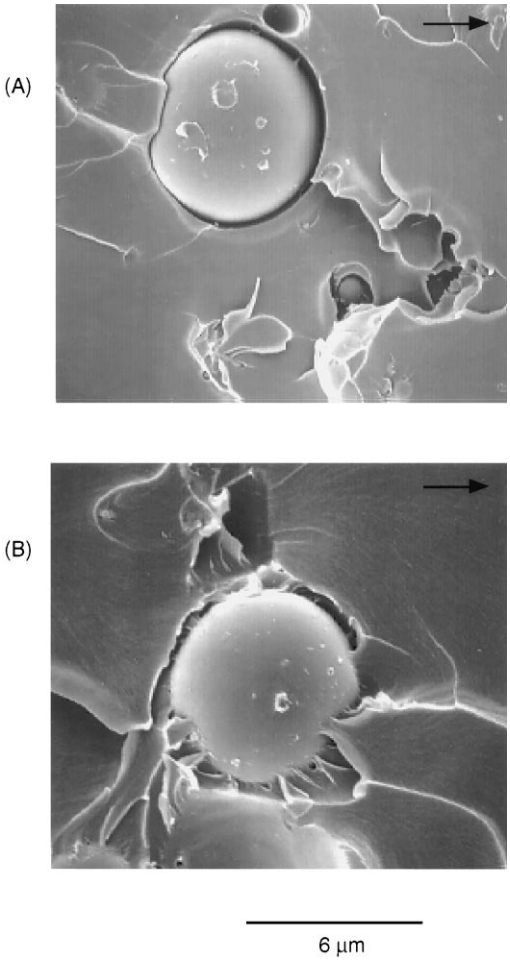

Fig. 7. SEM micrographs of the fracture surface (process zone) of SEN-3PB specimens of 10 vol% SG/661: (A) a typical micrograph of glass beads larger than 5–10 μm; (B) a typical micrograph of glass beads smaller than 5–10 μm. The arrows indicate the direction of crack propagation.

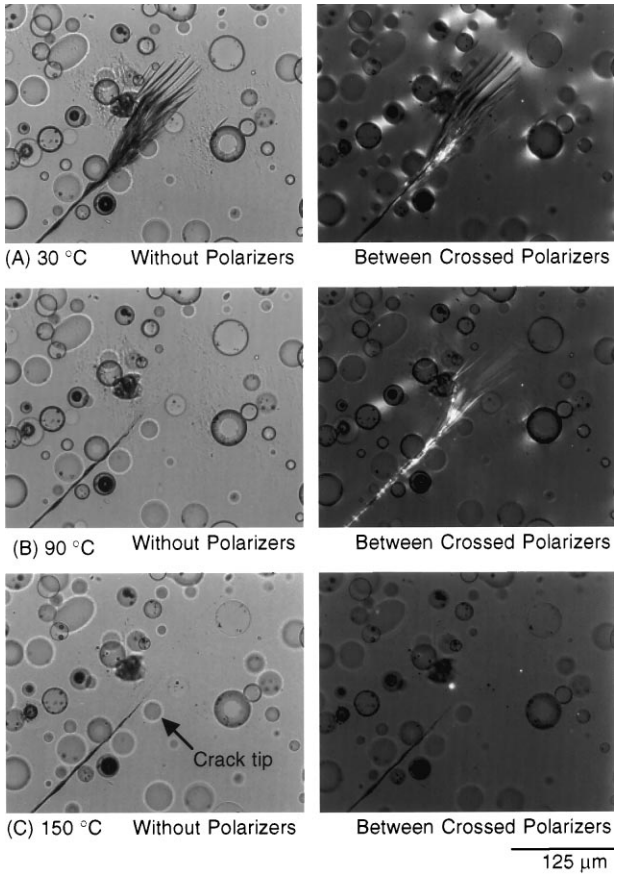

Fig. 8. Transmitted light optical micrographs of a sub-critically loaded crack in a DEN-4PB specimen of 10 vol% LG/667 (T_g of matrix = 99°C) taken without (left three micrographs) or between (right three micrographs) crossed polarizers: (A) at 30°C before heating; (B) at 90°C during heating at 0.5°C/min; and (C) at 150°C.

micro-shear (MS) bands exist at crack tip regions. This is shown in Figs. 8–11. Fig. 8(A) shows the dark line structures developed extensively at the crack tip. When these structures were first found in our experiment, they were thought to be microcracks instead of MS bands. Possible reasons are given in a subsequent section.

MS bands are usually birefringent [9,62,63], yet they are shown in Fig. 8(A). Even though polarized light is used, the birefringence of the line structures is not obvious. They are not crazes either, because crazing is unlikely to occur in the highly cross-linked thermosets used in this experiment [38,39,55]. Furthermore, it has been reported [55] that, in DDS-cured bisphenol A epoxies, as the cross-link density of the epoxies decreased, the major deformation mechanism of the epoxies changed from shear yielding to microcracking, not to crazing.

A heating experiment proved that the line structures are not microcracks. Fig. 8 shows the OM micrographs taken during heating of a thin-section at 0.5°C/min. At 90°C, which is still 9°C below the glass transition temperature (T_g) of matrix, the line structures are completely removed (Fig. 8(B)). When polarized light is used, birefringent lines become visible, which were not birefringent before heating. These birefringent lines can be removed by further heating as can be seen in the micrograph Fig. 8(C). It was also found that, once removed, the line structures were not restored even after cooling the thin-section to room temperature. From many heating experiments on thin-sections of different epoxies, it was concluded that the dark line structures found at crack tip regions or in process zones could be removed by thermal energy at a temperature below the T_g of the epoxy matrix.

If the dark line structures are microcracks, the thermal energy is not enough to remove them. To remove (heal) microcracks, usually temperature higher than T_g and pressure are needed [64–66]. Below the T_g of the matrix, the interdiffusion rates of macromolecular chains are too low to heal microcracks. Furthermore, the matrices used in this study were not thermoplastics but thermosets. In thermosets, macromolecular chains are anchored by chemical cross-links. Therefore, their interdiffusion rate must be much lower than that of thermoplastics. Moreover, the restoration of chemical cross-links in epoxy matrices is impossible at a temperature below T_g (90°C in Fig. 8). Accordingly, crack healing cannot occur during the heating experiments, so the results of heating experiments show that the dark lines must be something other than microcracks.

Not all of the dark lines found in thin-sections can be removed. Fig. 9 shows the dark lines found in fractured tensile specimens. Their positions and directions are more irregular than the line structures in SEN-3PB and DEN-4PB specimens. The most distinct difference between the two

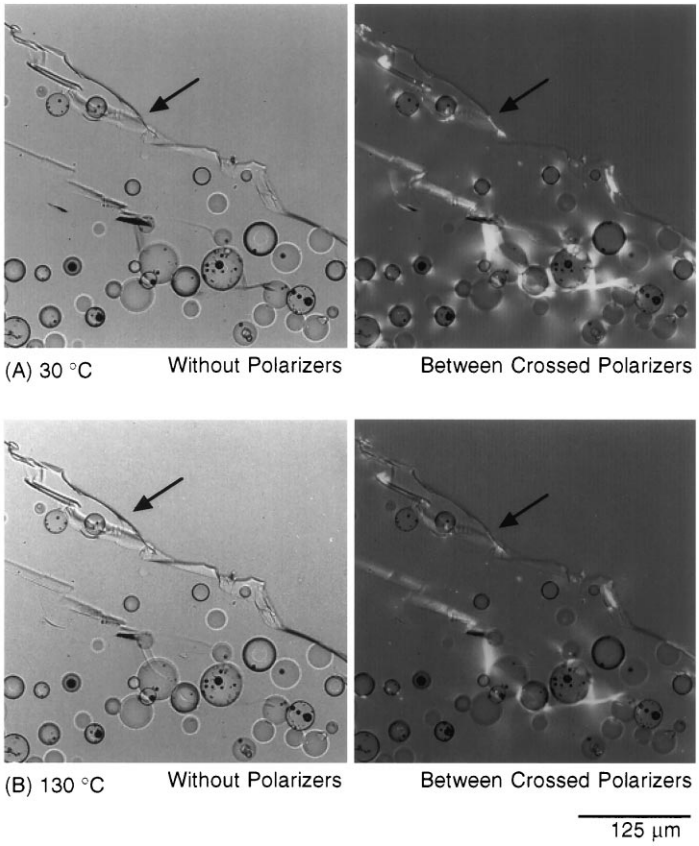

Fig. 9. Transmitted light optical micrographs of a thin section taken in a tensile specimen of 10 vol% LG/661 (T_g of matrix = 124°C): (A) at 30°C before heating; and (B) at 130°C during heating at 0.5°C/min. The arrows indicate the fracture surface.

line structures is the fact that the lines found in fractured tensile specimens cannot be removed by heating. In Fig. 9(B), even after heating above the T_g of the matrix, the lines are still apparent. In contrast to the lines found in SEN-3PB specimens, these lines are likely to be microcracks. It can also be noticed by examining the micrographs in Fig. 9 that the birefringence of shear bands and thermal residual misfit becomes weaker by heating.

To conclusively identify the dark line structures found in the crack tip regions, SEM and TEM microscopy were used. If the dark lines are microcracks or crazes that can appear as dark lines in the OM micrographs of thin sections, they will be observed in one of microscopy studies or both. Since it was reported [66] that crazes in thermoplastics could be removed by heating below T_g of materials, the heating experiment alone cannot be conclusive evidence for MS banding.

As illustrated in Fig. 10, a DEN-4PB specimen containing a sub-critically loaded crack was cryofractured, and the sub-critically loaded crack tip region was observed by SEM. Fig. 10(A) shows neither microcracks nor crazes around the crack tip (note the size of dark lines in Fig. 8). Only a single primary crack can be found in this micrograph. A total of more than 15 specimens were cryofractured and investigated, and not a single microcrack or craze was found in all the specimens. Fig. 10(B) shows a typical TEM micrograph of a sub-critically loaded crack tip. Similar to the SEM micrograph, this TEM micrograph shows a single crack tip without showing any microcracks or craze structures. More than 5 microtomed sections were investigated using TEM, and more than 10 microtomed sections were investigated using OM to confirm the result of Fig. 10(B). All these results confirm that the dark line structures found in the crack tip regions are MS bands.

The MS bands in Fig. 8 do not show any significant birefringence. Although polarized light is normally able to pass through shear yielded regions, their birefringence can be obscure if the angle between the shear bands and light path is not near zero. Refraction by the yielded regions is able to make MS bands look dark. Upon heating, the angle or width of MS bands can be changed due to relaxation. The refraction will also decrease. In a thin section, the removal of MS bands will first occur near the surface of sections. Thus, the shape of MS bands can be changed by heating,

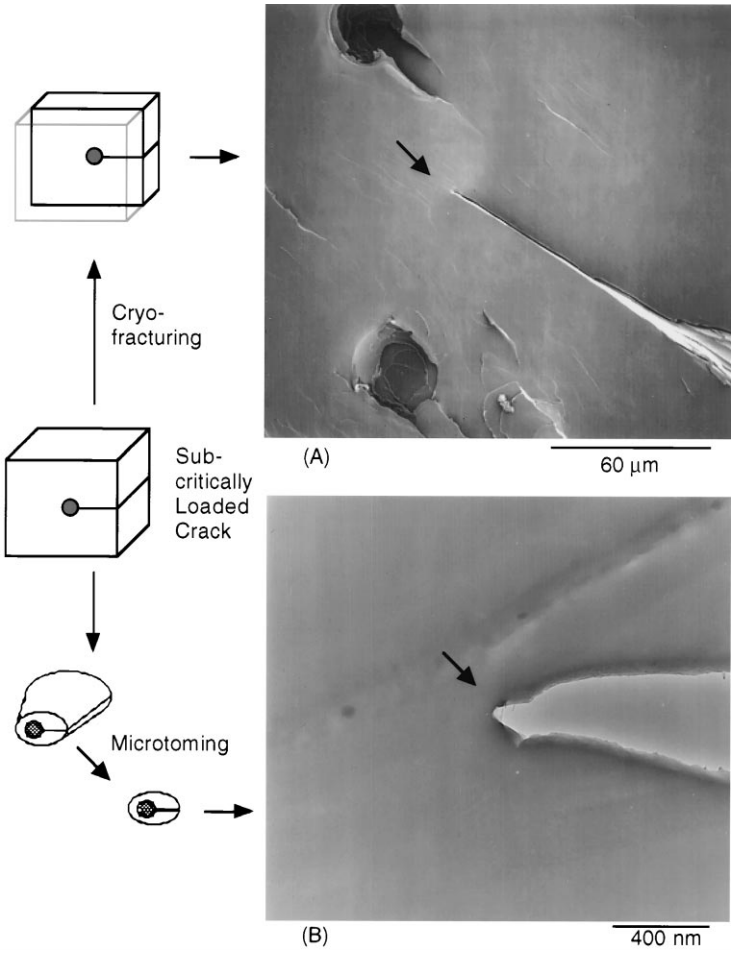

Fig. 10. No microcracks or crazes can be found in the tip regions of sub-critically loaded cracks in DEN-4PB specimens: (A) SEM micrograph of a 10 vol% LG/664 specimen cryofractured perpendicular to initial crack plane; (B) TEM micrograph of a 10 vol% LG/667 specimen microtomed perpendicular to initial crack plane. The arrows indicate the tips of sub-critically loaded cracks.

resulting in the birefringence of yielded regions becoming visible. However, these explanations, though plausible, need future verification. It is also unclear whether a dark line is a single MS band or a composite of many even thinner MS bands. If the width of the thinner bands is much narrower than the wavelength of the light, MS bands will have the appearance of dark lines instead of birefringent bands.

3.5. Summary of micro-mechanical deformations

Using various microscopy techniques, the important micro-mechanical deformations occurring during the fracture of glass bead filled epoxies were identified, and their characteristics were examined in this current study and also our previous studies [10–13]. The results of the microscopy studies are summarized in Fig. 11 as schematic illustrations of the three groups of glass bead filled epoxies: (1) low glass bead content and good interfacial strength between glass beads and the matrix; (2) low glass bead content and poor interfacial strength; and (3) high glass bead content regardless of the degree of interfacial strength.

In Fig. 11(A) (when glass bead content is less than 10 vol% in our experiment), the primary crack front first stays in an array of glass beads, and upon loading, MS bands develop around the glass beads in the crack tip region. In addition to MS banding, debonding of glass beads and DS yielding of matrix occur as well. Before the next array of glass beads debonds or the primary crack front propagates stably to the next array, the crack front starts to propagate unstably (catastrophically) at a critical stress. As a result, both debonding/DS zone and MS band zone are confined within a very narrow region containing an array of glass beads. After fracture, step structures including characteristic tails are left on the fracture surface.

As the interfacial strength decreases without increasing glass bead content, the size of debonding/DS zone increases, as shown in Fig. 11(B). Before it propagates unstably, the primary crack front can get to the next array of glass beads. On the other hand, the size of MS band zone does not change significantly. It can be expected that MS banding is triggered before debonding of glass beads occurs and propagates into the matrix. Therefore, MS banding seems to occur independently of the debonding process. In fact, since isolated MS bands can be found around the bonded glass beads ahead of crack tip in the previous OM micrographs (Fig. 8(A)), stress concentrations due to the existence of glass beads in the epoxy matrix appear to be sufficient to initiate MS banding. After a free (plane stress condition) surface is generated by debonding, DS yielding become the preferred mode of deformation [10–13]. Consequently, the decrease of interfacial strength facilitates the debonding of glass beads, resulting in increasing the debonding/DS yielding zone size, but not MS band zone size.

In the case of Fig. 11(C), which has high glass bead content, the process zone contains more than an array of

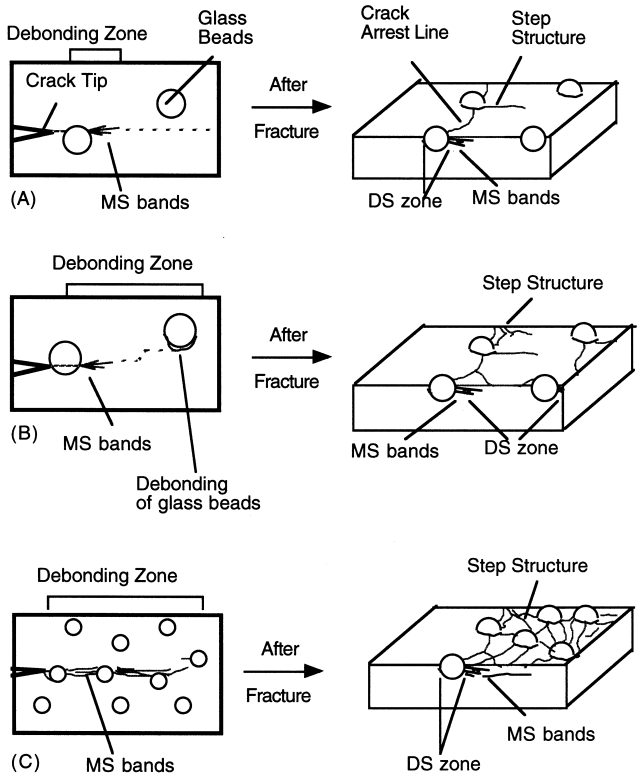

Fig. 11. Schematic illustration of fracture process in glass bead filled epoxies: (A) low glass bead content and good interfacial adhesion; (B) low glass bead content and poor interfacial adhesion; and (C) high glass bead content. All cracks in here propagate from left to right. (MS = micro-shear, DS = diffuse shear).

debonded glass beads regardless of the degree of interfacial strength. A large MS band zone develops between glass beads ahead of the crack tip. In the case of Fig. 11(C), step structures on fracture surface are quite intense and complex. Their directions are more irregular, indicating the very complicated directions of local crack propagation.

4. Conclusions

Micro-mechanical deformations occurring in the fracture of glass bead filled epoxies were investigated by using various microscopy techniques. The fracture processes of glass bead filled epoxies were identified. Three kinds of the major micro-mechanical deformations were observed: (1) step formation; (2) debonding of glass beads/DS yielding of matrix; and (3) MS banding.

On the fracture surface of glass bead filled epoxies, several types of steps such as characteristic tails behind glass beads, crack arrest lines, basic longitudinal textures, ‘lances’, etc, were observed. While the basic longitudinal texturing was found to be rather insensitive to the existence of glass beads, all the other step formations were.

From OM studies on sub-surface damage, it was found that debonding of glass beads and microcracking in the

matrix seldom occurred beneath the fracture surface. Microcracks in glass beads were also not generally found. The contribution of the combined process, debonding/DS yielding, to toughening can be larger than that of step formation. However, this process was found not to occur extensively. It was found that larger debonding zone size resulted with decreasing the interfacial strength between glass beads and matrix.

MS bands were clearly identified by a heating experiment and direct observations using SEM and TEM. It may be plausible that this deformation process could dissipate the large amount of fracture energy.

Acknowledgements

This work was supported by the Specialized Materials Science Research Center of National Institute of Health (NIH), under a contract No. DEO 9296-09. The authors would like to thanks Dr Jimmy Kishi and Dr Jack Huang for their help.

References

[1] Rothon R. Particulate-filled polymer composites. New York: Longman, 1995.
[2] Nielsen LE, Landel RF. Mechanical properties of polymers and composites. 2nd ed. New York: Marcel Dekker, 1994.
[3] Lange FF. Philos Mag 1970;22:983.
[4] Evans AG. Philos Mag 1972;26:1327.
[5] Green DJ, Nicholson PS, Embury JD. J Mater Sci 1977;12:987.
[6] Green DJ, Nicholson PS, Embury JD. J Mater Sci 1979;14:1413.
[7] Green DJ, Nicholson PS, Embury JD. J Mater Sci 1979;14:1657.
[8] Rice JR, Ben-Zion Y, Kim K. J Mech Phys Solids 1994;42:813.
[9] Kinloch AJ, Young RJ. Fracture behavior of polymers. Amsterdam: Elsevier, 1985.
[10] Lee J. PhD Thesis, The University of Michigan, 1998.
[11] Lee J, Yee AF. Polym Prepr, Am Chem Soc Div Polym Chem 1997;38:369.
[12] Lee J, Yee AF. Polym Prepr, Am Chem Soc Div Polym Mater 1998;79:200.
[13] Lee J, Yee AF. Polymer, 2000, to be published.
[14] Pearson RA, Yee AF. J Mater Sci 1986;21:2475.
[15] Holik AS, Kambour RP, Hobbs SY, Fink DG. Microstruct Sci 1979;7:367.
[16] Sawyer LC, Grubb DT. Polymer microscopy. New York: Chapman and Hall, 1987.
[17] Covavisaruch JS, Robertson RE, Filisko FE. J Mater Sci 1992;27:990.
[18] Nichols ME, Robertson RE. J Mater Sci 1994;29:5916.
[19] Reeves AA. Thesis MS, Dartmouth College, 1990.
[20] Williams JG. Fracture mechanics of polymers. 1st edn. Chichester, UK: Ellis Horwood, 1984.
[21] Azimi HR, Pearson RA, Hertzberg RW. Polym Engng Sci 1996;36:2352.
[22] Evans AG, Fu Y. Acta Metall 1985;33:1525.
[23] Evans AG, Williams S, Beaumont PWR. J Mater Sci 1985;20:3668.
[24] Avnir D, Biham O, Lidar D, Malcai O. Science 1998;279:39.
[25] Hansen A, Hinrichsen EL, Maloy KJ, Roux S. Phys Rev Lett 1993;71:204.
[26] Spanoudakis J, Young RJ. J Mater Sci 1984;19:473.
[27] Spanoudakis J, Young RJ. J Mater Sci 1984;19:487.
[28] Sommer E. Engng Fract Mechan 1969;1:539.
[29] Purslow D. Composites 1986;17:289.
[30] Atsuta M, Turner DT. J Mater Sci 1982;1:167.
[31] Kinloch AJ, Gilbert D, Shaw SJ. Polym Commun 1985;26:290.
[32] Hull D. Int J Fract 1993;62:119.
[33] Hull D. Int J Fract 1995;70:59.
[34] Hull D. J Mater Sci 1996;31:1829.
[35] Hull D. J Mater Sci 1996;31:4483.
[36] Mijovic J, Koutsky JA. Polymer 1979;20:1095.
[37] Lange FF, Lambe KAD. Philos Mag 1968;18:129.
[38] Donald AM, Kramer EJ. J Mater Sci 1981;16:2967.
[39] Donald AM, Kramer EJ. Philos Mag A 1981;43:857.
[40] Lauterwasser BD, Kramer EJ. Philos Mag A 1979;39:469.
[41] Robertson RE, Mindroiu VE. J Mater Sci 1985;20:2801.
[42] Moloney AC, Kausch HH, Kaiser T, Beer HR. J Mater Sci 1987;22:381.
[43] Vekinis G, Beaumont PWR, Pritchard G, Wainwright P. J Mater Sci 1991;26:4527.
[44] Hecht E. Optics. Reading, MA: Addison-Wesley, 1987.
[45] Brown SK. Br Polym J 1980:24.
[46] Evans AG, Faber KT. J Am Ceram Soc 1983;67:255.
[47] Rose LRF. J Am Ceram Soc 1986;69:212.
[48] Yee AF, Pearson RA. J Mater Sci 1986;21:2462.
[49] Yee AF, Li D, Li X. J Mater Sci 1993;28:6392.
[50] Li D, Yee AF, Chen IW, Chang SC, Takahashi K. J Mater Sci 1994;29:2205.
[51] Clyne TW, Withers PJ. An introduction to metal matrix composites. New York: Cambridge University, 1993.
[52] Wang CH. Engng Fract Mech 1997;56:77.
[53] Wang JS, Suo Z. Acta Metall 1990;38:1279.
[54] Atkinson C, Smelser RE, Sanchez J. Int J Fract 1982;18:279.
[55] Glad MD, Kramer EJ. J Mater Sci 1991;26:2273.
[56] Grenier-Loustalot M, Grenier P. Polymer 1992;33:1187.
[57] Hong SG, Lin JJ. J Polym Sci B 1997;35:2063.
[58] Gent AN. J Mater Sci 1980;15:2884.
[59] Pukanszky B, Van Es M, Maurer FHJ, Voros G. J Mater Sci 1994;29:2350.
[60] Cho K, Gent AN. J Mater Sci 1988;23:141.
[61] Zhong XA, Knauss WG. J Engng Mater Technol 1997;119:199.
[62] Argon AS, Andrews RD, Godrick JA, Whitney W. J Appl Phys 1968;39:1899.
[63] Kau C, Tse A, Hiltner A, Baer E. J Mater Sci 1993;28:529.
[64] Kausch HH, Petrovska D, Landel RF, Monnerie L. Polym Engng Sci 1987;27:149.
[65] Davies P, Cantwell W, Kausch HH. J Mater Sci 1989;8:1247.
[66] Schirrer R, Goett C. Int J Fract 1980;16:R133.